Title	Photonic crystal nanocavity with a Q factor exceeding eleven million
Author(s)	Asano, Takashi; Ochi, Yoshiaki; Takahashi, Yasushi; Kishimoto, Katsuhiro; Noda, Susumu
Editor(s)	
Citation	Optics Express. 2017, 25 (3), p.1769-1777
Issue Date	2017-02-06
URL	http://hdl.handle.net/10466/15719
Rights	(c) 2017 Optical Society of America. Users may use, reuse, and build up on the article, or use the article for text or data mining, so long as such uses are for non-commercial purposes and appropriate attribution is maintained. All other rights are reserved.

Research Article | Vol. 25, No. 3 | 6 Feb 2017 | OPTICS EXPRESS 1769
Optics EXPRESS

Photonic crystal nanocavity with a *Q* factor exceeding eleven million

TAKASHI ASANO,[1,*] YOSHIAKI OCHI,[1] YASUSHI TAKAHASHI,[2] KATSUHIRO KISHIMOTO,[1] AND SUSUMU NODA[1,3]

[1]*Department of Electronic Science and Engineering, Kyoto University, Kyoto 615-8510 Japan*
[2]*Department of Physics and Electronics, Osaka Prefecture University, Sakai, Osaka 599-8570, Japan*
[3]*Photonics and Electronics Science and Engineering Center, Kyoto University, Kyoto 615-8510 Japan*
[*]*tasano@qoe.kuee.kyoto-u.ac.jp*

Abstract: Photonic crystal nanocavities that simultaneously possess small modal volumes and high quality (*Q*) factors have opened up novel research areas in photonics during this decade. Here, we present an important key for the increase of *Q* factors to ranges beyond ten million. A systematic investigation on photon lifetimes of air-bridge-type heterostructure nanocavities fabricated from silicon on insulator (SOI) substrates indicated the importance of cleaning the bottom side (buried oxide side) of the nanaocavites. Repeated thermal oxidation and an oxide removal process applied after the removal of the buried oxide layer underneath the nanocavities realized an experimental *Q* factor greater than eleven million, which is the highest experimental *Q* ever recorded. The results provide important information not only for Si PC nanocavities but also for general Si nanophotonic devices and photonic electronic convergence systems.

OCIS codes: (230.5298) Photonic crystals; (230.5750) Resonators.

References and links

1. R. D. Meade, A. Devenyi, J. D. Joannopoulos, O. L. Alerhand, D. A. Smith, and K. Kash, "Novel applications of photonic band gap materials: Low-loss bends and high Q cavities," J. Appl. Phys. **75**(9), 4753–4755 (1994).
2. O. Painter, R. K. Lee, A. Scherer, A. Yariv, J. D. O'Brien, P. D. Dapkus, and I. Kim, "Two-dimensional photonic band-Gap defect mode laser," Science **284**(5421), 1819–1821 (1999).
3. S. Noda, A. Chutinan, and M. Imada, "Trapping and emission of photons by a single defect in a photonic bandgap structure," Nature **407**(6804), 608–610 (2000).
4. K. Srinivasan and O. Painter, "Momentum space design of high-Q photonic crystal optical cavities," Opt. Express **10**(15), 670–684 (2002).
5. Y. Akahane, T. Asano, B.-S. Song, and S. Noda, "High-Q photonic nanocavity in a two-dimensional photonic crystal," Nature **425**(6961), 944–947 (2003).
6. B. S. Song, S. Noda, T. Asano, and Y. Akahane, "Ultra-high-Q photonic double-heterostructure nanocavity," Nat. Mater. **4**(3), 207–210 (2005).
7. D. Englund, I. Fushman, and J. Vucković, "General recipe for designing photonic crystal cavities," Opt. Express **13**(16), 5961–5975 (2005).
8. T. Asano, B.-S. Song, and S. Noda, "Analysis of the experimental Q factors (~ 1 million) of photonic crystal nanocavities," Opt. Express **14**(5), 1996–2002 (2006).
9. E. Kuramochi, M. Notomi, S. Mitsugi, A. Shinya, T. Tanabe, and T. Watanabe, "Ultrahigh- Q photonic crystal nanocavities realized by the local width modulation of a line defect," Appl. Phys. Lett. **88**(4), 041112 (2006).
10. Y. Takahashi, H. Hagino, Y. Tanaka, B. S. Song, T. Asano, and S. Noda, "High-Q nanocavity with a 2-ns photon lifetime," Opt. Express **15**(25), 17206–17213 (2007).
11. E. Kuramochi, H. Taniyama, T. Tanabe, A. Shinya, and M. Notomi, "Ultrahigh-Q two-dimensional photonic crystal slab nanocavities in very thin barriers," Appl. Phys. Lett. **93**(11), 111112 (2008).
12. Z. Han, X. Checoury, D. Néel, S. David, M. El Kurdi, and P. Boucaud, "Optimized design for 2×10^6 ultra-high Q silicon photonic crystal cavities," Opt. Commun. **283**(21), 4387–4391 (2010).
13. Y. Taguchi, Y. Takahashi, Y. Sato, T. Asano, and S. Noda, "Statistical studies of photonic heterostructure nanocavities with an average Q factor of three million," Opt. Express **19**(12), 11916–11921 (2011).
14. M. Minkov, U. P. Dharanipathy, R. Houdré, and V. Savona, "Statistics of the disorder-induced losses of high-Q photonic crystal cavities," Opt. Express **21**(23), 28233–28245 (2013).
15. H. Sekoguchi, Y. Takahashi, T. Asano, and S. Noda, "Photonic crystal nanocavity with a Q-factor of ~9 million," Opt. Express **22**(1), 916–924 (2014).

#281833 http://dx.doi.org/10.1364/OE.25.001769
Journal © 2017 Received 5 Dec 2016; revised 13 Jan 2017; accepted 13 Jan 2017; published 23 Jan 2017

16. Y. Lai, S. Pirotta, G. Urbinati, D. Gerace, M. Minkov, V. Savona, A. Badolato, and M. Galli, "Genetically designed L3 photonic crystal nanocavities with measured quality factor exceeding one million," Appl. Phys. Lett. **104**(24), 241101 (2014).
17. T. Nakamura, Y. Takahashi, Y. Tanaka, T. Asano, and S. Noda, "Improvement in the quality factors for photonic crystal nanocavities via visualization of the leaky components," Opt. Express **24**(9), 9541–9549 (2016).
18. Z. Zhang and M. Qiu, "Small-volume waveguide-section high Q microcavities in 2D photonic crystal slabs," Opt. Express **12**(17), 3988–3995 (2004).
19. H.-S. Ee, K.-Y. Jeong, M.-K. Seo, Y.-H. Lee, and H.-G. Park, "Ultrasmall square-lattice zero-cell photonic crystal laser," Appl. Phys. Lett. **93**(1), 011104 (2008).
20. M. Nomura, Y. Ota, N. Kumagai, S. Iwamoto, and Y. Arakawa, "Zero-cell photonic crystal nanocavity laser with quantum dot gain," Appl. Phys. Lett. **97**(19), 191108 (2010).
21. U. P. Dharanipathy, M. Minkov, M. Tonin, V. Savona, and R. Houdré, "High-Q silicon photonic crystal cavity for enhanced optical nonlinearities," Appl. Phys. Lett. **105**(10), 101101 (2014).
22. B.-S. Song, S.-W. Jeon, and S. Noda, "Symmetrically glass-clad photonic crystal nanocavities with ultrahigh quality factors," Opt. Lett. **36**(1), 91–93 (2011).
23. Z. Han, X. Checoury, L.-D. Haret, and P. Boucaud, "High quality factor in a two-dimensional photonic crystal cavity on silicon-on-insulator," Opt. Lett. **36**(10), 1749–1751 (2011).
24. K. K. Mehta, J. S. Orcutt, O. Tehar-Zahav, Z. Sternberg, R. Bafrali, R. Meade, and R. J. Ram, "High-Q CMOS-integrated photonic crystal microcavity devices," Sci. Rep. **4**, 4077 (2014).
25. M. Lončar, A. Scherer, and Y. Qiu, "Photonic crystal laser sources for chemical detection," Appl. Phys. Lett. **82**(26), 4648–4650 (2003).
26. S. Kita, K. Nozaki, and T. Baba, "Refractive index sensing utilizing a cw photonic crystal nanolaser and its array configuration," Opt. Express **16**(11), 8174–8180 (2008).
27. T. Yoshie, A. Scherer, J. Hendrickson, G. Khitrova, H. M. Gibbs, G. Rupper, C. Ell, O. B. Shchekin, and D. G. Deppe, "Vacuum Rabi splitting with a single quantum dot in a photonic crystal nanocavity," Nature **432**(7014), 200–203 (2004).
28. K. Hennessy, A. Badolato, M. Winger, D. Gerace, M. Atatüre, S. Gulde, S. Fält, E. L. Hu, and A. Imamoğlu, "Quantum nature of a strongly coupled single quantum dot-cavity system," Nature **445**(7130), 896–899 (2007).
29. Y. Ota, S. Iwamoto, N. Kumagai, and Y. Arakawa, "Spontaneous two-photon emission from a single quantum dot," Phys. Rev. Lett. **107**(23), 233602 (2011).
30. S. Strauf, K. Hennessy, M. T. Rakher, Y.-S. Choi, A. Badolato, L. C. Andreani, E. L. Hu, P. M. Petroff, and D. Bouwmeester, "Self-tuned quantum dot gain in photonic crystal lasers," Phys. Rev. Lett. **96**(12), 127404 (2006).
31. M. Nomura, N. Kumagai, S. Iwamoto, Y. Ota, and Y. Arakawa, "Laser oscillation in a strongly coupled single quantum dot-nanocavity system," Nat. Phys. **6**(4), 279–283 (2010).
32. A. Faraon, A. Majumdar, D. Englund, E. Kim, M. Bajcsy, and J. Vučković, "Integrated quantum optical networks based on quantum dots and photonic crystals," New J. Phys. **13**(5), 055025 (2011).
33. Y. Tanaka, J. Upham, T. Nagashima, T. Sugiya, T. Asano, and S. Noda, "Dynamic control of the Q factor in a photonic crystal nanocavity," Nat. Mater. **6**(11), 862–865 (2007).
34. S. Matsuo, A. Shinya, T. Kakitsuka, K. Nozaki, T. Segawa, T. Sato, Y. Kawaguchi, and M. Notomi, "High-speed ultracompact buried heterostructure photonic-crystal laser with 13 fJ of energy consumed per bit transmitted," Nat. Photonics **4**(9), 648–654 (2010).
35. Y. Takahashi, Y. Inui, M. Chihara, T. Asano, R. Terawaki, and S. Noda, "A micrometre-scale Raman silicon laser with a microwatt threshold," Nature **498**(7455), 470–474 (2013).
36. K. Nozaki, A. Shinya, S. Matsuo, Y. Suzaki, T. Segawa, T. Sato, Y. Kawaguchi, R. Takahashi, and M. Notomi, "Ultralow-power all-optical RAM based on nanocavities," Nat. Photonics **6**(4), 248–252 (2012).
37. Y. Sato, Y. Tanaka, J. Upham, Y. Takahashi, T. Asano, and S. Noda, "Strong coupling between distant photonic nanocavities and its dynamic control," Nat. Photonics **6**(1), 56–61 (2011).
38. R. Konoike, H. Nakagawa, M. Nakadai, T. Asano, Y. Tanaka, and S. Noda, "On-demand transfer of trapped photons on a chip," Sci. Adv. **2**(5), e1501690 (2016).
39. R. Terawaki, Y. Takahashi, M. Chihara, Y. Inui, and S. Noda, "Ultrahigh-Q photonic crystal nanocavities in wide optical telecommunication bands," Opt. Express **20**(20), 22743–22752 (2012).
40. M. Borselli, T. J. Johnson, and O. Painter, "Measuring the role of surface chemistry in silicon microphotonics," Appl. Phys. Lett. **88**(13), 131114 (2006).
41. E. Yablonovitch, D. L. Allara, C. C. Chang, T. Gmitter, and T. B. Bright, "Unusually low surface-recombination velocity on silicon and germanium surfaces," Phys. Rev. Lett. **57**(2), 249–252 (1986).
42. T. Takahagi, I. Nagai, A. Ishitani, H. Kuroda, and Y. Nagasawa, "The formation of hydrogen passivated silicon single-crystal surfaces using ultraviolet cleaning and HF etching," J. Appl. Phys. **64**(7), 3516–3521 (1988).
43. L. Ling, Z. J. Radzimski, T. Abe, and F. Shimura, "The effect of bonded interface on electrical properties of bonded silicon-on-insulator wafers," J. Appl. Phys. **72**(8), 3610–3616 (1992).
44. J. I. Furihata, M. Nakano, and K. Mitani, "Heavy-metal (Fe/Ni/Cu) behavior in ultrathin bonded silicon-on-insulator (SOI) wafers evaluated using radioactive isotope tracers," Japanese J. Appl. Physics, Part 1 Regul. Pap. Short Notes Rev. Pap. **39**(4) B, 2251–2255 (2000).
45. D. Gui, Y. N. Hua, Z. X. Xing, and S. P. Zhao, "Investigation of potassium contamination in SOI wafer using dynamic SIMS," IEEE Trans. Device Mater. Reliab. **7**(2), 369–372 (2007).

Optics EXPRESS

1. Introduction

Photonic nanocavities based on artificial defects in two-dimensional (2D) photonic crystal (PC) slabs [1–3] have recently realized extremely high quality (Q) factors in the range of tens of thousands to millions or more together with small modal volumes (V) of the order of one cubic wavelength or less. Because such photonic nanocavities can concentrate electromagnetic energy in both space and frequency domains, they are one of the most important tools to manipulate photons, and are widely used in various scientific and engineering fields. There have been various efforts to increase the Q factors of 2D-PC slab nanocavities both in theory and experiment [4–17]. Methods to maximize of Q/V [18–21] and those to obtain high Q factors without using air-bridge structures [22–24] have been also intensively studied.

Meanwhile, the realization of nanocavities with Q factors greater than thousands leads to development of low threshold nanolasers [19, 20, 25, 26] which can be used for high-performance material sensing. The development of nanocavities with Q factors greater than tens of thousands [5] realized strongly coupled light-matter systems in solid [27–29], a few and single quantum dot(s) lasers [30, 31], quantum-logic gates [32], on-demand catch/release of photons [33], etc. Furthermore, nanocavities with Q factors greater than hundreds of thousands enabled exotic photon manipulation technologies including ultra-low threshold InP-b/InGaAsP [34] and Si Raman [35] lasers, ultra-low-power consumption optical bistable systems [36], strong coupling of distant nanocavities [37] with adiabatic photon transfer [38], and the like. Further improvement of the Q factors will improve the performances of these techniques and also open up new frontiers in photon manipulation.

So far, the highest experimental Q factors (Q_{exp}) have been obtained in heterostructure-type Si slab nanocavities made from silicon-on-insulator (SOI) wafers [5, 6, 8–13, 15]. In general, Q_{exp} is determined by design, structural fluctuations, and optical absorptions, where the last factor is most difficult to investigate. In this connection, we recently reported that a remarkable increase of Q_{exp} was observed after dipping the nanocavities in dilute HF (DHF) to remove a thin oxide layer naturally formed on the Si surface; the best nanocavity showed a record Q_{exp} of nine million [15]. However, the average Q_{exp} obtained in that study was 4.4 million for six measured nanocavities [15], which is quite low compared to the highest Q_{exp} of nine million; the variance seems to be attributable to the instability of the natural oxidization process that depends on many complex parameters including humidity, temperature, storage time, and contamination.

In this paper, we present a systematic investigation of Q_{exp} of Si heterostructure-type nanocavities during several repetitions of controlled surface oxidization and oxide removal treatments. We show that it is important to clean the bottom side (buried oxide side) of the nanaocavites. This process stably reproduced an average Q_{exp} over 7.5 million, and realized the record highest Q_{exp} exceeding eleven million. These studies will provide important information not only for Si PC nanocavities but also for general Si nanophotonic devices and photonic electronic convergence systems.

2. Sample structure and experimental setup

Figure 1(a) shows a schematic of the 2D-PC slab heterostructure nanocavity studied in the current work. The PC consisted of a triangular lattice of circular air holes with radii of 110 nm, formed in a 220-nm-thick Si slab, where the base lattice constant a_1 is 410 nm. The nanocavity was formed by a line defect of 17 missing air holes where the lattice constant in the x-direction was increased from the center to outer every two periods by 3 nm twice as shown in Fig. 1(a). In addition, the blue air holes in Fig. 1(a) were shifted by $0.001a_1$ outward in the y-direction, and the red air holes were shifted by $0.002a_1$ outward in the x-direction; a leaky component visualization method [17] was used for the optimization of the design. The design Q factor (Q_{des}) and the modal volume were calculated by the three-dimensional finite-difference time-domain (3D-FDTD) method to be 1.3×10^8 and 1.4 cubic resonant

wavelengths in the material. An excitation waveguide which was 10%-wider than the cavity was prepared in parallel with the cavity, where the distance between them was six rows of air holes. The additional Q factor determined by the in-plane coupling to the excitation waveguide (Q_{in}) was calculated to be ~6×10^7 by the 3D FDTD method. Therefore, the actual Q_{des} was calculated to be 4×10^7 by including the load of Q_{in}.

The samples were fabricated on a SOI substrate prepared by Soitec using the Smart Cut method. The thickness of the top Si slab is 220 nm and that of the buried oxide (SiO_2) is 3000 nm. The top Si is doped with boron and its resistivity is 10 Ωcm, from which the doping density is estimated to be of the order of 1×10^{15} cm^{-3}. After defining the PC pattern by using electron beam lithography on the resist mask coated on the wafer, the pattern was transferred to the top Si slab by an inductively coupled plasma etching process using SF_6-based gas. The sample surface was cleaned by standard cleaning process for Si wafers, and by thin thermal oxidation with a subsequent removal of the surface oxide. The PC area was 300 μm × 15 μm, and nine nanocavities were placed along the excitation waveguide with a period of 20 μm, similar to those used in the previous reports [39]. One side of the waveguide end was cleaved to form an input facet for excitation light. We labeled the nanocavities as #1, #2, ..., #9 in ascending order of distance from the input facet. Finally, the buried oxide underneath the PC slab was removed by HF to form an air-bridge structure.

Figure 1(b) shows the measurement system used. Several modifications have been made from the previous study [15] in order to enable controlled oxidization. Samples were put on a sample stage equipped with a heater and thermocouple for oxidization at elevated temperatures up to 300°C. They were placed in an isolation chamber in which the ambient can be controlled by using dry inert gas (N_2 or Ar) or dry air. Excitation light was introduced in the chamber through an optical fiber of which end facet was shaped into a lens. The position of the optical fiber was aligned by a xyz-stage driven by actuators. We performed time-domain measurements as outlined in Fig. 1(b) to evaluate the lifetimes (τ) of photons trapped in the nanocavities: We excited a cavity by an optical pulse with a duration of 10 ns and measured the decay of photon emission from the cavity by the time-correlated single photon counting method. We evaluated τ from the later part of the decay curve in order to avoid influence of the tail of the excitation pulse (see Fig. 2). The Q_{exp} of the nanocavity was estimated according to the relation $Q_{exp} = \omega\tau$, where ω is the resonant frequency. Details of the measurement have been described previously [10]. It is noteworthy that samples were always kept in a dry ambient, except for the processes that required chamber opening (for example, the DHF treatment described below). The chamber wall and sample stage were baked at 80°C and 300°C, respectively, in vacuum for more than one week, before starting the measurement.

Optics EXPRESS

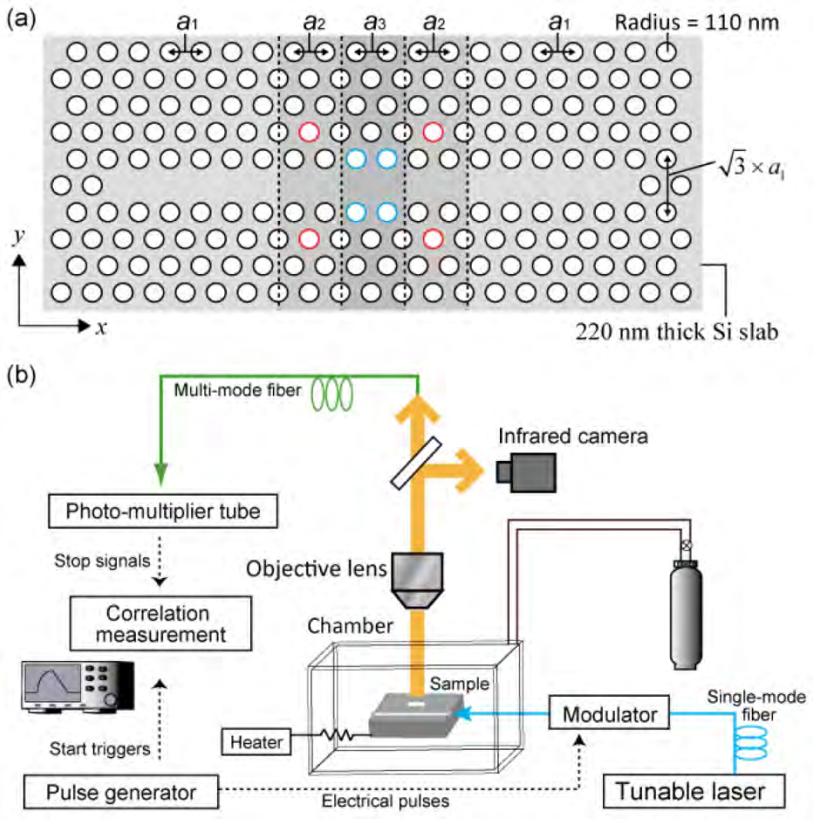

Fig. 1. (a) Structure of the heterostructure nanocavity used in the experiment. (b) Optical measurement setup.

3. Experimental results

The experiment was carried out as follows: After the fabrication of a sample with a final dipping into HF to remove the buried oxide, the sample was placed in the measurement chamber filled with a dry inert gas (N_2 or Ar), and Q_{exp} values of the nanocavities were measured. Next, the sample was oxidized within the measurement chamber in dry air ambient at an elevated temperature. Q_{exp} values of the nanocavities were evaluated after the sample had cooled down to room temperature. The sample was taken out from the measurement chamber, dipped into DHF, rinsed with de-ionized water, and dried by blowing with dry N_2. The sample was returned to the chamber within 15 min after the DHF process and Q_{exp} values were evaluated in dry inert gas ambient. This procedure was repeated four times to check the stability.

Figure 2 shows the photon lifetime curve of one of the prepared nanocavities (#6) just after fabrication, that after the first oxidization process, and that after the first DHF process. It is seen in the figure that τ decreased from 5.2 ns to 3.9 ns after the oxidization and increased to 6.2 ns after the DHF treatment. The corresponding Q_{exp} values are 6.3, 4.7, and 7.5 million, respectively. Simultaneously, the resonant wavelength changed from 1567.5 nm to 1567.26 nm and 1565.30 nm for each treatment step. The blue shifts of the resonant wavelength are caused by the decrease of the refractive index by surface oxidization, and the decrease of the slab volume by oxide removal. The total blue shift of the resonant wavelength (2.2 nm) observed for this process corresponds to the uniform removal of silicon at the cavity surface (including inner walls of the air holes) by about 0.5 nm according to the 3D-FDTD calculation. The decrease of τ after the oxidization is due to the formation of interface states

at the Si/SiO_2 interface [40], and the increase of τ after oxide removal is attributed to the removal of the interface states and termination of the Si surface with hydrogen [15, 40–42]. More importantly, one cycle of this treatment increased τ or Q_{exp} by 19%, which demonstrates the effectiveness of this cleaning method. The changes of Q_{exp} and the resonant wavelength of nanocavity #6 through the four repetitions of the above procedure are presented in Table 1. (Here, the maximum Q_{exp} measured after the process is shown, but, in fact, Q_{exp} slowly changes over a few days.) It is seen in the table that Q_{exp} started from 6.3 million, reached to 9.1 million after the second oxidization /DHF treatment, and kept almost 9 million for the subsequent repetition of oxidization /DHF treatments.

We can discuss the reason for the increase of Q_{exp} from several features seen in Table 1: (A) Q_{exp} after the first oxidization (4.7 million) is different from than those after the second, third, and fourth oxidizations (3.6 ~3.9 million). (B) Q_{exp} after the first oxidization/DHF treatment (7.5 million) is less than those after the second ~fourth oxidization/DHF treatments (~9 million). (C) The blue shift of the resonant wavelength after the first oxidization (0.25 nm) is much less than those for the second ~fourth oxidizations (0.9~1.1 nm). These features clearly indicates the situation in the first oxidization/DHF treatment is different from that in the subsequent oxidization/DHF treatments. We suspect influence of the bottom side (buried oxide side) surface of the Si slab: The state of the bottom side surface just after the fabrication is considered to be different from those for the top surface and the inner walls of the air holes because the latter two surfaces already experienced the cleaning processes that includes thermal oxidization and oxide removal during the fabrication while the bottom side surface was always covered with buried oxide that was not removed until the final step of the fabrication. The interface between the top Si and buried oxide can concentrate contamination [43–45], which can remain after the removal of the buried oxide by HF. It is considered that the oxidization/DHF treatment applied after the removal of buried oxide reduced contaminants at the bottom side surface of the nanocavity and drastically improved Q_{exp}.

Table 2 represents Q_{exp} of the 9 prepared nanocavities measured 2 days after the second oxidization/DHF and 5 days after the fourth oxidization/DHF process. It is noted that the controlled oxidization and oxide removal process can consistently reproduce very high Q_{exp}. High Q_{exp} values greater than 6 million were obtained for 8 of the nanocavities in both measurements, and an extremely high average $Q_{exp} > 7.5$ million is obtained. (We could not determine the resonance of nanocavity #2.) This average Q_{exp} is 60% larger than the previous value of 4.4 million [15]. The relatively smaller Q_{exp} observed after the fourth process is probably due to the longer storage time after the DHF process or fluctuations in the oxidization/DHF process.

Figure 3 shows the longest photon lifetime curves that were obtained for nanocavity #8 just after the fourth oxidization/DHF processes. It can be seen in the figure that a very long photon lifetime of 9.2 ns, which corresponds to a Q factor of 11 million (1.11×10^7), is obtained experimentally. This is a record-breaking Q factor—the highest ever reported for 2D-PC nanocavities. The decay rate did not change for the estimated input power range used here, which indicates that nonlinear effects—especially two-photon absorption—are negligibly small. The Q factor decreased to 9.9 million five days after this measurement (as shown in Table 2) even though the sample was kept in a dry inert gas (N_2) ambient.

Optics EXPRESS

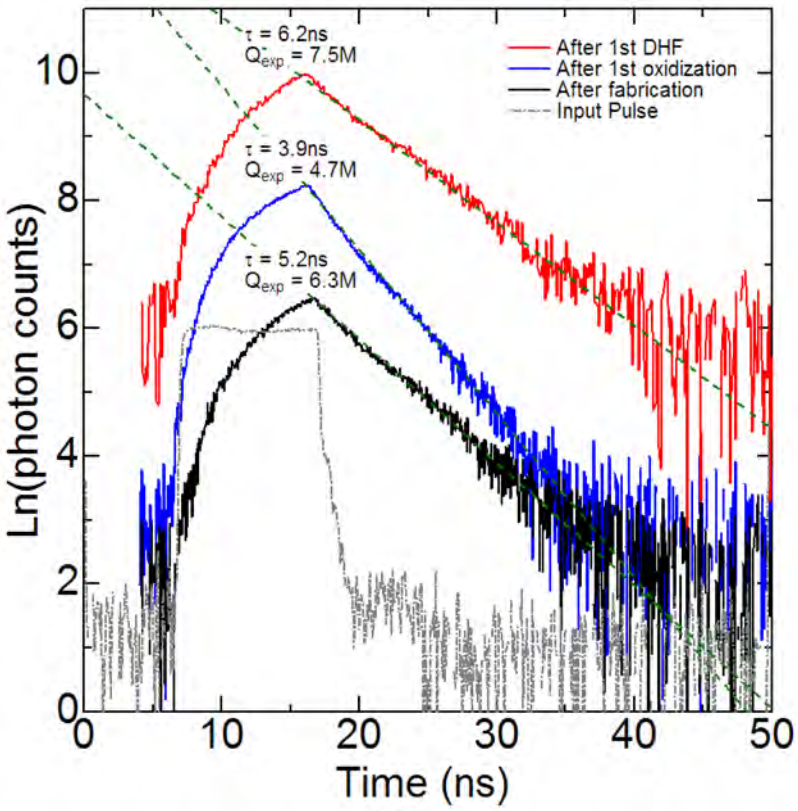

Fig. 2. Decay curves of photons in a nanocavity (#6 presented in Table 2) just after the fabrication (black solid line), after the first oxidization process (blue solid line), and after the subsequent oxide removal (DHF) process (red solid line). The cavity is excited by an input pulse with a width of 10 ns (gray dashed line). The small dip at around 20 ns is attributed to the influence of the tail of the input pulse. We evaluated photon lifetimes (τ) from the later part (>25 ns) of the decay curves.

Table 1. Change of experimental *Q* factor (Q_{exp}), resonant wavelength, and shift of resonant wavelength of a nanocavity through four cycles of oxidization (OX) and DHF processing. The maximum Q_{exp} measured after the process is shown. The sample is nanocavity #6 presented in Table 2.

Process	Resonant Wavelength (nm)	Resonant Wavelength Shift (nm)	Q_{exp} (million)
After fabrication	1567.5 ± 0.1	-	6.2
OX #1	1567.26	–0.25	4.7
DHF #1	1565.33	–1.96	7.5
OX #2	1564.41	–0.89	3.6
DHF #2	1562.39	–2.02	9.1
OX #3	1561.49	–0.91	3.9
DHF #3	1559.05	–2.32	8.8
OX#4	1558.04	–1.12	3.8
DHF#4	1555.85	–2.16	9.1

Table 2. Experimental *Q* factors of 9 nanocavities measured 2 days after the 2nd oxidization (OX)/DHF process and 5 days after the 4th OX/DHF process. Statistical

evaluations of losses are also shown. The labels Avg. and S.D. refer to the average and standard deviation, respectively. The mark "-" indicates that the resonance of the cavity could not be measured.

Cavity number	1	2	3	4	5	6	7	8	9	Avg. ($1/Q_{exp}$)	Avg. ($1/Q_{imp}$)	S.D. ($1/Q_{imp}$)
2 days after 2nd OX/DHF Q_{exp} ($\times 10^6$)	8.4	-	6.9	6.8	7.2	9.0	7.4	10.3	8.1	1.27×10^{-7}	1.0×10^{-7}	1.8×10^{-8}
5 days after 4th OX/DHF Q_{exp} ($\times 10^6$)	8.0	-	6.1	6.4	7.8	8.5	6.7	9.9	7.8	1.34×10^{-7}	1.1×10^{-7}	2.1×10^{-8}

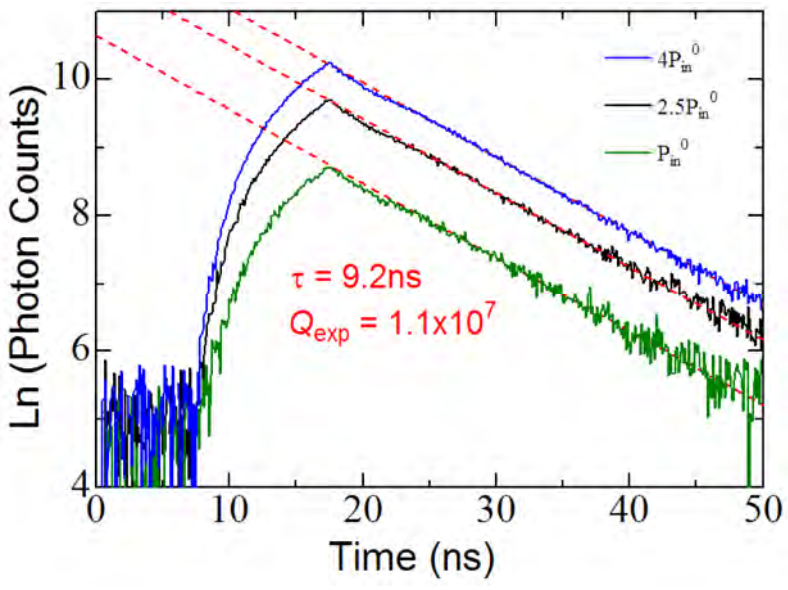

Fig. 3. Decay curve of photons in a nanocavity (#8) just after the 4th oxidization/DHF process. The cavity is excited by an input pulse with a width of 10 ns at various powers. We evaluated photon lifetimes from the later part (>25 ns) of the decay curves. The longest photon lifetime observed is 9.2 ns. Peak power of the input light within the excitation waveguide P_{in}^0 = 30 ~300 nW which depends on uncertain coupling efficiency at the input facet of the excitation waveguide.

As we reported before, insights into the origin of the loss due to the imperfections ($1/Q_{imp}$) can be obtained from the statistical analysis of Q_{exp} [13]. For this analysis, we first remove the loss determined by the design (Q_{des}) by using the following relation [8]:

$$\frac{1}{Q_{exp}} = \frac{1}{Q_{des}} + \frac{1}{Q_{imp}} \quad (1)$$

We used a Q_{des} value of 4×10^7, which was determined from the 3D-FDTD calculation including the load of the excitation waveguide. The evaluated average loss due to the imperfections [Avg.($1/Q_{imp}$)] and its standard deviation [S. D.($1/Q_{imp}$)] are presented in the two right-most columns of Table 2. Here, $1/Q_{imp}$ can be divided into scattering loss ($1/Q_{scat}$) and absorption loss ($1/Q_{abs}$) as follows:

$$\frac{1}{Q_{imp}} = \frac{1}{Q_{scat}} + \frac{1}{Q_{abs}} \quad (2)$$

$1/Q_{scat}$ is mainly determined by the fluctuations of the structure, and $1/Q_{abs}$ is determined by the light absorption of the material. We are able to calculate the magnitude of $1/Q_{scat}$ due to random air-hole variations using the FDTD simulations. In this calculation, random nanometer-scale variations in the positions and radii were applied to all the air holes in the calculation space in such a way that the probability of the variations followed a normal distribution with a standard deviation of σ_{hole} [13]. We performed the calculation for 30 different fluctuation patterns to obtain the statistical relationship between σ_{hole} (in nm) and Avg. $(1/Q_{scat})$, and σ_{hole} and S.D. $(1/Q_{scat})$ as follows [13]:

$$\text{Avg.}(1/Q_{scat}) = 7.5\times10^{-7}\times\sigma_{hole}^2 \quad (3)$$

$$\text{S.D.}(1/Q_{scat}) = 3.0\times10^{-7}\times\sigma_{hole}^2 \quad (4)$$

By assuming that the fluctuations of $1/Q_{imp}$ are mostly determined by the variation of air holes and that the fluctuation of absorption loss can be ignored, i.e. S.D.$(1/Q_{imp})$ = S.D.$(1/Q_{scat})$, we obtain σ_{hole} of 0.24 ~0.26 nm from the experimental S.D.$(1/Q_{imp})$ of 1.8 ~2.1 × 10^{-8} in Table 2 using Eq. (4). (Such small fluctuations in positions and radii of air holes are beyoud the observation accuracy of scanning electron microscopes.) When we put σ_{hole} = 0.25 nm into Eq. (3), experimental Avg.$(1/Q_{scat})$ is estimated to be 4.7 × 10^{-8}, and therefore experimental Avg.$(1/Q_{abs})$ is estimated to be ~5.8 × 10^{-8} using experimentally obtained Avg.$(1/Q_{imp})$ of 1.05 × 10^{-7} and Eq. (2). As a result, the ratio of the average contribution of $1/Q_{des}$, $1/Q_{scat}$, and $1/Q_{abs}$ to $1/Q_{exp}$ are estimated to be about 20%, 35%, and 45%, respectively. We think there is still room for improvement of Q_{exp} because the contribution of the design on the total loss is only 20%, but for that purpose, the origin of the absorption loss should be clarified. Possible origins are free-carriers supplied from surface stastes or residual impurities of the silicon slab.

Incidentally, Avg.$(1/Q_{abs})$ of 5.8 × 10^{-8} for the eight samples after the fourth *controlled* oxidization/DHF treatment is larger than Avg.$(1/Q_{abs})$ of 1.3 × 10^{-8} that we previously reported for the six samples with one application of *natural* oxidization/DHF treatment [15]. This is because we underestimated the value in the previous study due to the assumption that the fluctuation of $1/Q_{abs}$ should be negligible. As opposed to this assumption, the instability of the natural oxidization process could have caused the fluctuation of $1/Q_{abs}$. As a result, we overestimated S.D.$(1/Q_{scat})$ and σ_{hole}, which led to the evaluation of larger Avg.$(1/Q_{scat})$ and smaller Avg. $(1/Q_{abs})$. The instability can be also the origin for the smaller average Q_{exp} of 4.4 million, compared to the highest Q_{exp} of nine million, in the previous study [15].

4. Conclusion

We have successfully improved the experimental *Q* factors of air-bridge type Si-based 2D-PC nanocavities from the order of 4.4 million to over 7.5 million on average by cleaning the air-bridge structure using controlled dry oxidization and subsequent oxide removal by dilute HF. A record-high *Q* factor of 11 million was obtained immediately after the fourth cycle of this cleaning process. It is considered that the improvement of the bottom side (buried oxide side) of the Si slab accounts for this drastic improvement of *Q* factors. The fluctuations of radii and positions of air holes after this cleaning process have been evaluated to be < 0.25 nm by a statistical investigation. The contribution of design, scattering, and absorption to the experimental *Q* factors of the nanocavities is approximately 20%, 35%, and 45%, respectively. We believe that the high-*Q* nanocavities obtained in this report will stimulate various scientific and engineering fields.

Funding

JSPS KAKENHI (23360033 and 15H05428); New Energy and Industrial Technology Development Organization (NEDO).